

Measurement of the friction coefficient of a fluctuating contact line using an AFM-based dual-mode mechanical resonator*

Guo Shuo(郭 硕)^{a)}, Xiong Xiao-Min(熊小敏)^{b)}, Xu Zu-Li(徐祖力)^{a)},
Sheng Ping(沈 平)^{a)}, and Tong Peng'er(童彭尔)^{a)†}

^{a)}Department of Physics, Hong Kong University of Science and Technology, Clear Water Bay, Kowloon, Hong Kong, China

^{b)}Department of Physics and State Key Laboratory of Optoelectronic Materials and Technologies, Sun Yat-sen University, Guangzhou 510275, China

(Received 30 January 2014; published online 17 September 2014)

A dual-mode mechanical resonator using an atomic force microscope (AFM) as a force sensor is developed. The resonator consists of a long vertical glass fiber with one end glued onto a rectangular cantilever beam and the other end immersed through a liquid–air interface. By measuring the resonant spectrum of the modified AFM cantilever, one is able to accurately determine the longitudinal friction coefficient ξ_v along the fiber axis associated with the vertical oscillation of the hanging fiber and the traversal friction coefficient ξ_h perpendicular to the fiber axis associated with the horizontal swing of the fiber around its joint with the cantilever. The technique is tested by measurement of the friction coefficient of a fluctuating (and slipping) contact line between the glass fiber and the liquid interface. The experiment verifies the theory and demonstrates its applications. The dual-mode mechanical resonator provides a powerful tool for the study of the contact line dynamics and the rheological property of anisotropic fluids.

Keywords: contact line dynamics, atomic force microscope (AFM) resonator, friction coefficient, liquid interfaces

PACS: 68.05.–n, 07.79.–v, 83.10.Mj, 83.85.Vb

DOI: 10.1088/1674-1056/23/11/116802

1. Introduction

In recent years, there has been a growing interest in applying atomic force microscopy in liquid environments for studies of biomolecular structures,^[1] live cell manipulations,^[2] and dynamics near solid–liquid and liquid–liquid interfaces.^[3–6] When the atomic force microscope (AFM) cantilever is immersed in a liquid, its motion (e.g. oscillations in the tapping mode) is damped by the fluid viscosity. The piezo-electric shaker, which drives the mechanical motion of the cantilever, also generates different flow modes near the surface, which may in turn alter the resonance spectrum of the cantilever. A number of theoretical and numerical studies have been carried out aimed at understanding the mechanical response of small cantilevers of different shapes immersed in a viscous fluid.^[6–12] Experimental efforts were also made to find ways to increase the quality factor Q of the cantilever's resonant peak,^[7] such as by using active feedback circuits.^[13]

In a recent experiment,^[14] we designed a new AFM probe with a simple geometry to overcome the experimental difficulties. The modified AFM probe contains a long hanging glass fiber with one end glued to the front end of a rectangular cantilever beam and the other end immersed through a liquid–air interface. Because the cantilever beam is kept in air, the entire cantilever system acts as a mechanical resonator, which can accurately measure the viscous dissipations on the thin fiber

without introducing over-damping to the system. It was found that the vertical motion of the modified cantilever can be accurately described by the Langevin equation for a damped harmonic oscillator, from which we can obtain the friction coefficient ξ_v parallel to the long axis of the glass fiber as a function of the immersion length h into the liquid phase. The working principle of the single-mode mechanical resonator was thoroughly tested and the experiment demonstrated its applications.

In this paper, we report a further study of this mechanical resonator from being a single resonant mode to a dual-mode operation, which includes both the vertical oscillation of the cantilever and the horizontal swing of the glass fiber around the joint between the fiber and the cantilever. With the capability of simultaneously measuring the longitudinal friction coefficient ξ_v along the fiber axis and the traversal friction coefficient ξ_h perpendicular to the fiber axis, the dual-mode mechanical resonator provides a convenient and powerful tool for the study of the rheological property of anisotropic fluids, such as liquid crystals. The technique is also very useful for the study of the contact line dynamics, in which the contact line motion along the fiber axis is different from that perpendicular to the fiber axis. By comparing the two distinct behaviors between the longitudinal friction ξ_v and the traversal friction ξ_h , we identify a unique contribution of the fric-

*Project supported by the Research Grants Council of Hong Kong, China (Grant Nos. 605013, 604211, and SRFI11/SC02) and the National Natural Science Foundation of China (Grand Nos. 10974259 and 11274391).

†Corresponding author. E-mail: peng'er@ust.hk

tion coefficient ξ_v^c associated with a fluctuating (and slipping) contact line between the glass fiber and the liquid interface. Furthermore, by varying the liquid viscosity η by almost two decades, we find that the contact line dissipation obeys a scaling law, $\xi_v^c = \alpha \pi d \eta$, where πd is the contact line length, and $\alpha = 1.82 \pm 1$, which does not change much with the liquid–solid contact angle. This universal scaling law, applicable to liquids with different viscosities, surface tensions, and contact angles, establishes a rigorous relationship that can be used to test various microscopic models for the moving contact line.

The remainder of the paper is organized as follows. We first describe the basic working principle of the dual-mode mechanical resonator in Section 2. The apparatus and the experimental method are discussed in Section 3. The experimental results are discussed in Section 4, and the work is summarized in Section 5. A primary objective of this paper is to delineate the experimental conditions for the precise measurement of the friction coefficient associated with a fluctuating contact line, which has been a difficult classical problem.

2. Theory

We consider a modified cantilever for an AFM as shown in Fig. 1(a). The top end of a thin glass fiber is glued onto a rectangular cantilever beam, and the other end of the vertical fiber touches a liquid–air interface, at which a circular contact line between the interface and the fiber surface is formed. The hanging fiber cantilever system acts as a mechanical resonator,^[14] which oscillates vertically with a resonant frequency f_i . By using the AFM setup shown in Fig. 1(b), one can accurately record the vertical displacement of the cantilever (\equiv vertical deflection of the cantilever). As a three-dimensional (3D) object, the hanging fiber cantilever system has a number of resonant modes. Figures 2(a) and 2(b) show the two low-frequency resonant modes of the hanging fiber cantilever system: (a) vertical oscillation of the cantilever and (b) horizontal swing of the hanging fiber around its joint point with the cantilever.

In the vertical oscillation mode, the cantilever oscillates vertically with the hanging fiber following the vertical motion passively, and there is no relative conformational change between the fiber and the cantilever. In the horizontal swing mode, however, the hanging fiber swings horizontally around the joint between the fiber and the cantilever, which can also produce a local vertical deformation at the further end of the cantilever. This oscillation mode is different from the vertical oscillation mode of the entire cantilever with the other end fixed by the cantilever holder. It will be shown below that these two oscillation modes can be treated as two independent eigenmodes of the hanging fiber cantilever system.

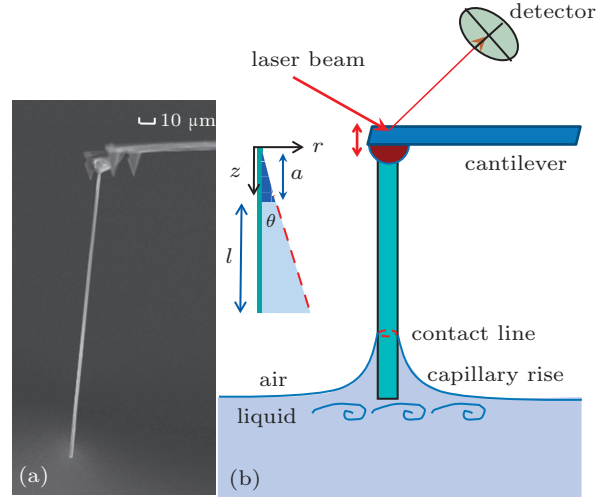


Fig. 1. (a) A modified AFM cantilever with a hanging glass fiber of diameter $d = 4 \mu\text{m}$ and length $L = 280 \mu\text{m}$. The top end of the glass fiber is glued onto a rectangular cantilever beam. (b) Sketch of the AFM-based hanging fiber resonator and the capillary rise around the fiber tip. The inset shows the geometry near the contact line and the coordinate system used in Eq. (12).

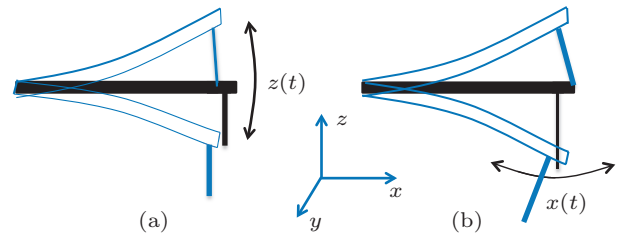


Fig. 2. Sketch of two low-frequency resonant modes of the hanging fiber cantilever system: (a) vertical oscillation of the cantilever beam and (b) horizontal swing of the glass fiber around the glue joint.

To investigate the resonant spectrum of the modified cantilever, we calculate the eigenfrequencies of the hanging fiber cantilever system using the actual dimensions and material parameters given in Table 1. The numerical calculation is carried out by solving the linear elasticity equation for the displacement vector field $\mathbf{u}(\mathbf{x}, t)$ ^[15]

$$\rho \frac{\partial^2 \mathbf{u}}{\partial t^2} = \nabla \cdot [\mathbf{C} : \boldsymbol{\varepsilon}], \quad (1)$$

where ρ is the mass density, \mathbf{C} is the fourth-order stiffness tensor, and $\boldsymbol{\varepsilon} = (1/2)[\nabla \mathbf{u} + (\nabla \mathbf{u})^T]$ is the displacement induced strain tensor field. For isotropic materials to be used in the experiment, \mathbf{C} has a simple form

$$\mathbf{C} = B \begin{bmatrix} 1-\nu & \nu & \nu & 0 & 0 & 0 \\ \nu & 1-\nu & \nu & 0 & 0 & 0 \\ \nu & \nu & 1-\nu & 0 & 0 & 0 \\ 0 & 0 & 0 & \frac{1-2\nu}{2} & 0 & 0 \\ 0 & 0 & 0 & 0 & \frac{1-2\nu}{2} & 0 \\ 0 & 0 & 0 & 0 & 0 & \frac{1-2\nu}{2} \end{bmatrix}, \quad (2)$$

where $B = E/[(1+\nu)(1-2\nu)]$, with E being the Young's modulus and ν the Poisson ratio; both are material parameters.

Table 1. Physical dimensions of the cantilever, glass fiber, and UV curable glue used in the experiment and their material properties, including Young's modulus E , Poisson ratio ν , and mass density ρ .

Physical dimensions	Cantilever (rectangular)	Glass fiber (cylindrical)	Glue (semi-spherical)
length $L/\mu\text{m}$	130	270	
width $W/\mu\text{m}$	35	2	10
height $H/\mu\text{m}$	2	radius	radius
Material properties	silicon	glass	NOA 81
E/GPa	131	73.1	1.38
ν	0.27	0.17	0.043
$\rho/\text{kg}\cdot\text{m}^{-3}$	2330	2203	1150

Table 2. Obtained first three (or two) eigenfrequencies of the three objects: (i) a single rectangular cantilever beam orientated horizontally with one end fixed, (ii) a single cylindrical glass fiber orientated vertically with its top end fixed, and (iii) the combined fiber plus cantilever system shown in Fig. 1(b).

Eigenfrequencies /kHz	Cantilever alone		Glass fiber alone		Cantilever plus glass fiber	
	numerical	analytical	numerical	analytical	numerical	experimental
f_1	145.2	143.6	44.2	44.3	34.1	32.7
f_2	907.4	898.6	276.9	277.2	105.9	102
f_3	2387.1	2512.7				

In fact, one can obtain the analytic solutions of the eigenfrequencies of the first two objects (i) and (ii) by solving a simpler elastic equation^[8]

$$\rho \frac{\partial^2 u(x,t)}{\partial t^2} + \frac{EI}{A} \frac{\partial^4 u(x,t)}{\partial x^4} = 0 \quad (3)$$

for the deflection $u(x,t)$ of the cantilever (or fiber) along its length x with one end (at $x = 0$) fixed and under no external force. Here I is the second moment of inertia and A is the cross-sectional area of the cantilever (or fiber). The final result for the i th eigenfrequency is

$$f_i = \frac{\alpha_i}{2\pi} \sqrt{\frac{EI}{\rho AL^4}}, \quad (4)$$

where L is the total length of the cantilever (or fiber), $\alpha_1 = 3.52$, $\alpha_2 = 22.03$, and $\alpha_3 = 61.70$. For a rectangular beam of width W and thickness H , its second moment of inertia is given by $I = WH^3/12$, and for a cylinder of radius R one has $I = \pi R^4/4$. The analytical results for the first two objects are also given in Table 2. The shapes of the cantilever (or fiber) corresponding to the three resonant frequencies have been described in Ref. [16]. From Table 2, one finds that the numerical results agree with the analytical results for the first two objects, indicating that our numerical setup works well.

The motion of the combined fiber plus cantilever system in a liquid environment can be described by the Langevin equation^[12,14]

$$m \frac{\partial^2 z}{\partial t^2} + \xi \frac{\partial z}{\partial t} + kz = f_B(t), \quad (5)$$

where $z(t)$ is the vertical deflection of the cantilever, $\xi \partial z/\partial t$ is the drag force on the glass fiber with ξ being the friction coef-

The numerical calculation is carried out by solving Eqs. (1) and (2) for three elastic objects: (i) a single rectangular cantilever beam orientated horizontally with one end fixed, (ii) a single cylindrical glass fiber orientated vertically with its top end fixed, and (iii) the combined fiber plus cantilever system shown in Fig. 1(b). The physical dimensions and the material properties of the three objects are given in Table 1. The numerical model is implemented using the COMSOL Multiphysics software package. Table 2 gives the first three (or two) eigenfrequencies obtained for the three objects.

cient, $kz(t)$ is the elastic force due to the bending of the cantilever with a spring constant k , and $f_B(t)$ is the random Brownian force due to thermal fluctuations of the surrounding fluid. The mean value of $f_B(t)$ is zero, but its auto-correlation function, $C(\tau) = \langle f_B(t+\tau)f_B(t) \rangle$, is non-zero and has the form^[17]

$$C(\tau) = 2k_B T \xi \delta(\tau), \quad (6)$$

where $k_B T$ is the thermal energy of the system and $\delta(\tau)$ is the δ function.

The measurable quantity in the experiment is the power spectrum, $|z(\omega)|^2$, of the vertical deflections of the cantilever (or equivalently $|z(f)|^2$), which can be solved analytically from Eqs. (5) and (6) as^[12,14]

$$|z(\omega)|^2 = \frac{2k_B T \xi / m^2}{(\omega^2 - \omega_0^2)^2 + (\omega \xi / m)^2}, \quad (7)$$

where $\omega = 2\pi f$ is the angular frequency and $\omega_0 = (k/m)^{1/2}$ is the resonant frequency of the system. In a previous experiment,^[14] we thoroughly tested Eq. (7) using a long glass fiber with only one resonant mode (vertical mode) excited. The experiment demonstrated that the motion of the hanging glass fiber at the interface can indeed be described by Eq. (7) very accurately.

Because equation (5) is a linear equation, its solution will be a superposition of two resonant peaks; each can be described by Eq. (7) when the system has two resonant modes as depicted in Fig. 2. In this case, we will have two resonant frequencies $\omega_{0i} = \sqrt{k_i/m_i}$ and two friction coefficients ξ_i . In the following, we will use the two subscripts v and h to indicate (i) the vertical oscillation of the cantilever and (ii) the horizontal swing of the glass fiber, respectively.

3. Experiment

Figure 1(a) shows a modified cantilever with a hanging glass fiber 4 μm in diameter and 270 μm in length viewed under a microscope. The thin glass fiber is pulled from a glass rod 2 mm in diameter and 100 mm in length using a pipette puller (model P-97, Sutter Instrument Co.). The thin glass fiber is then glued to the further end of the rectangular cantilever beam using a UV curable glue (Norland, NOA 81). As shown in Fig. 1(a), the fiber is tilted at an angle of 11° with respect to the cantilever normal so that the hanging fiber becomes normal to the liquid–air interface when the cantilever is mounted on the AFM holder. Commercial silicon microcantilevers (MikroMasch) with spring constant k in the range of 2–16 N/m are used in the experiment. Finally, the glass fiber is cut to a desired length using a pair of homemade sharp tweezers. The entire assembly process is carried out with the help of a motorized micromanipulator system together with a high-magnification stereo microscope (Leica MZ16).

The liquid–air interface is prepared using a stainless steel cell 10 mm in diameter and 5 mm in depth. The top of the cell has a sharp circular edge, which is used to pin the liquid–air interface in order to reduce unwanted surface flow. The diameter of the cell is chosen to be not too small so that the water–air interface can be kept flat visually. It should also be not too large in order to reduce unwanted surface motion. The entire stainless steel cell is mounted inside a closed AFM fluid cell purchased from Asylum Research Inc. Prior to each measurement, the sample cell is thoroughly cleaned following the same procedures as described in Ref. [14]. A stepper motor is used to move the fluid cell upward with an accuracy of 0.1 μm . When the tip of the glass fiber touches the liquid–air interface, a large change in the cantilever deflection is detected by an AFM sensor due to the capillary force, making the determination of the contact point between the fiber tip and the liquid–air interface accurate within 0.1 μm . In the experiment, the hanging fiber remains stationary and the interface is moved upward towards the glass fiber in steps of 1 μm . The immersion length h of the glass fiber into the liquid–air interface (see Fig. 1(b)) can be varied in the range of 0.1–300 μm .

Measurements of the power spectrum $|z(f)|^2$ are conducted using an AFM (MFP-3D, Asylum Research Inc.) operated under the thermal power spectral density (PSD) mode. Under this mode, the voltage signal from the position-sensitive detector (see Fig. 1(b)) is digitized at a sampling frequency of 5 MHz. Typically, $|z(f)|^2$ is taken with a frequency resolution of 152 Hz and the averaging time for each $|z(f)|^2$ at a fixed value of h is set to 2–5 min. To determine the absolute value of $|z(f)|^2$, the output voltage signal from the position-sensitive detector is calibrated against known values of the cantilever deflection. This is done for all the modified cantilevers with a hanging glass fiber, using the procedure provided by the AFM

manufacturer. It is found that the experimental uncertainties of the measured $|z(f)|^2$ can be kept at the level of 5%–10%.

To study the horizontal swing mode as shown in Fig. 2(b), one needs to find the coupling constant β , which connects the horizontal displacement Δx of the fiber tip to the vertical displacement Δz of the cantilever via the equation $\Delta z = \beta \Delta x$ (for small Δx). In the experiment, a stripe-shaped silicon wafer (MikroMasch TGZ11), as sketched in Fig. 3, is used to calibrate the horizontal displacement of the hanging fiber. The hanging fiber first moves vertically toward the silicon wafer until the fiber tip touches the wafer substrate. It then moves horizontally across the substrate surface. The vertical displacement of the cantilever shows a stick–slip-like motion due to the unevenness of the substrate surface. When the fiber tip is in the groove region and is just in contact with the strip sidewall, the fiber starts to bend horizontally while the cantilever bends vertically. Both the fiber’s horizontal movement Δx and the cantilever’s forced vertical displacement Δz are recorded by the AFM. The obtained Δz is found to be a linear function of Δx for small values of Δx and the coupling constant β is obtained from the slope $\Delta z/\Delta x$. Using the physical parameters given in Table 1, we also calculate the value of β numerically using the theoretical model described in Section 2. The numerical result is $\beta = 0.072$, which is close to the measured value $\beta = 0.084$.

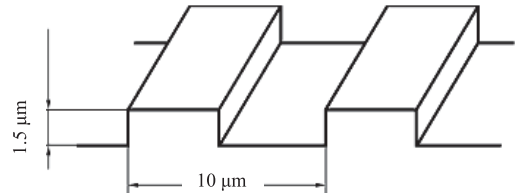


Fig. 3. A stripe-shaped silicon wafer used for the calibration of the horizontal displacement of the hanging fiber. The wafer substrate has a step of height 1.5 μm and period 10 μm .

4. Experimental results

4.1. Two low-frequency resonant modes of the hanging fiber probe

Figure 4 compares the measured power spectra $|z(f)|^2$ as a function of f for a bare cantilever before adding the glass fiber (black dashed line) and the modified cantilever with a hanging fiber of diameter $d = 4 \mu\text{m}$. For the bare cantilever, only a single resonant peak associated with the vertical oscillation of the cantilever appears in the power spectrum. After adding the hanging glass fiber, two resonant peaks appear in the measured $|z(f)|^2$: a low frequency peak located at $\sim 30 \text{ kHz}$ and a high frequency peak located at $\sim 100 \text{ kHz}$. The high frequency peak results from the vertical oscillation of the cantilever and its resonant frequency is shifted downward because of the increase in mass. The low frequency peak

results from the horizontal swing of the glass fiber around the glue joint.

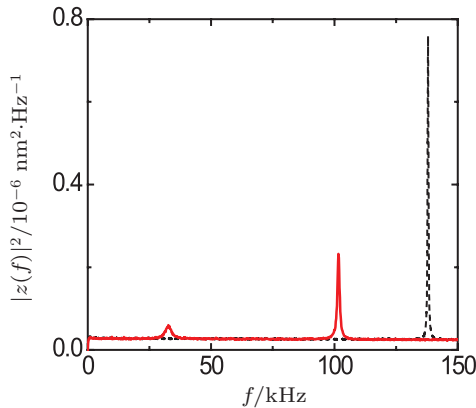


Fig. 4. Comparison of the measured $|z(f)|^2$ between a bare cantilever (black dashed line) and the modified cantilever with a hanging glass fiber of diameter $d = 4 \mu\text{m}$ (red solid line). The measurements are made in air. The two peak positions agree well with the predictions obtained numerically (see text).

Table 3. Calculated horizontal resonant frequency f_h and vertical resonant frequency f_v as a function of fiber length L and diameter d .

$L/\mu\text{m}$ (for $d = 4 \mu\text{m}$)	f_h/kHz	f_v/kHz	$d/\mu\text{m}$ (for $L = 270 \mu\text{m}$)	f_h/kHz	f_v/kHz
135	179.1	86.9	1	10.9	121.4
200	55.9	124.9	2	21.7	111.5
270	33.5	80.8	4	34.1	105.9
400	16.8	105.9	6	31.3	111.2
540	9.7	92.2	8	25.6	108.1

To further verify the new features of the measured $|z(f)|^2$, we conduct a numerical calculation of the eigenfrequencies of the combined fiber–cantilever system shown in Fig. 1(a). Using the physical parameters given in Table 1 and the COMSOL Multiphysics software package, we obtain the first two eigenfrequencies, which are given in Table 2. By carefully examining the resonant shape of the combined fiber–cantilever system, we find that the first eigenfrequency corresponds to the horizontal swing mode of the glass fiber, as depicted in Fig. 2(b). This frequency is smaller than f_1 for the glass fiber alone, because the fiber end connected to the cantilever is not fixed stationary in this case. The second eigenfrequency is found to be associated with the vertical oscillation mode of the cantilever beam, as depicted in Fig. 2(a). This frequency is slightly smaller than f_1 for the cantilever alone, because the effective mass of the combined fiber–cantilever system is increased. It is seen from Table 2 that the numerical results agree well with the two measured resonant frequencies with errors less than 5%. Figure 4 thus demonstrates that the motion of the combined fiber–cantilever system can indeed be described by two independent harmonic oscillators with an effective mass m_i , friction coefficient ξ_i , and spring constant k_i , as shown in Fig. 2.

From the assembly of the combined fiber–cantilever system, we find that the UV curable glue and the geometry of the glass fiber play a critical role in magnifying the small resonant peak associated with the horizontal swing mode of the glass fiber. Either reducing the amount of glue or pushing the glass fiber too close to the cantilever beam will diminish the small low frequency peak. To make sure that the cantilever can adequately feel the horizontal swing of the fiber, the amount of glue between the fiber tip and the cantilever beam should be kept as large as possible. This is consistent with our numerical finding that a semisphere of glue between the fiber tip and the cantilever beam (see Fig. 1(b)) is needed to obtain numerical and experimental agreement. It is also found that, to have two resonant peaks measurable in the power spectrum, the ratio of the fiber length to its diameter should be kept at ~ 70 and the fiber diameter cannot be too small ($d \gtrsim 2 \mu\text{m}$). When the length-to-diameter ratio becomes larger than 100, the measured $|z(f)|^2$ has only one resonant peak, corresponding to the vertical vibration of the cantilever. In addition, the glass fiber should be aligned perpendicular to the cantilever beam under a microscope, so that there is no other unwanted resonant mode excited in the wide frequency range, as shown in Fig. 4.

Using the physical parameters given in Table 1 and the COMSOL Multiphysics software package, we also investigate how the resonant frequencies f_v associated with the vertical oscillation of the cantilever and f_h associated with the horizontal swing of the fiber change with the fiber length L and diameter d . Table 3 summarizes the final numerical results. It is seen from Table 3 that f_v does not change much with the fiber dimensions. The horizontal resonant frequency f_h , however, is very sensitive to the change of the fiber dimensions. If the fiber is too long ($> 500 \mu\text{m}$) or too thin ($< 1 \mu\text{m}$), f_h will become too small to be distinguished from the low frequency noise in the surroundings. In this case, the coupling constant β discussed in Section 3 will also become very small, making the detection of the horizontal swing mode of the fiber from the vertical deflection of the cantilever difficult.

Figure 5 shows how the measured $|z(f)|^2$ changes when the hanging fiber is pushed through the water–air interface at different immersion lengths h . Once in touch with the water–air interface, the frequency peaks change continuously with increasing damping (i.e. with increasing value of h); the frequency peaks broaden while the peak heights decrease and the peak positions shift to lower frequencies. This behavior agrees with the prediction shown in Eq. (7). Figure 5 thus demonstrates that the measured $|z(f)|^2$ is very sensitive to the viscous damping and one can use this sensitivity to study the hydrodynamics near liquid–air interfaces.

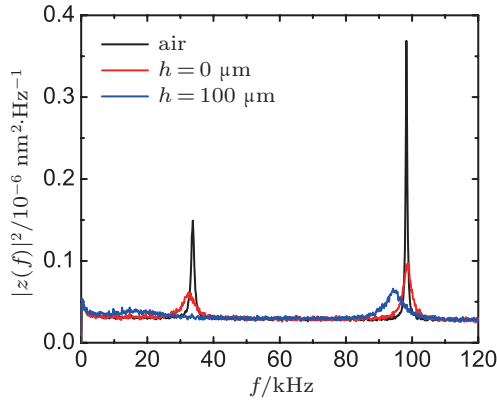


Fig. 5. Evolution of the measured $|z(f)|^2$ when the glass fiber is pushed through a water–air interface at different immersion lengths (from right to left): in air (black curve), $h = 0 \mu\text{m}$ (just in touch with the interface, red curve), and $h = 100 \mu\text{m}$ (blue curve).

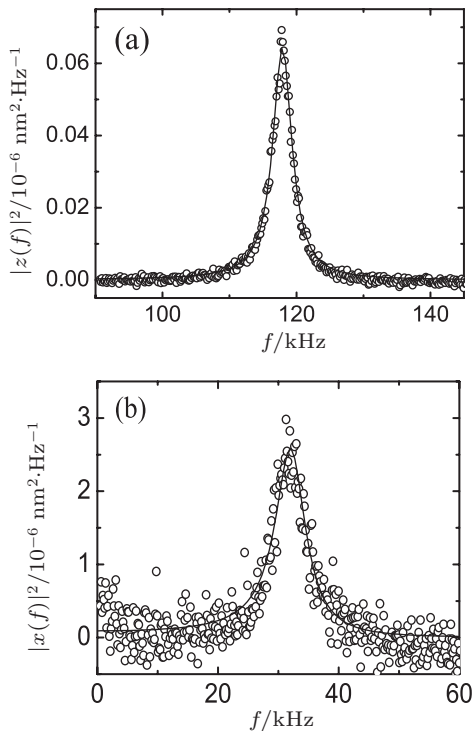


Fig. 6. (a) A magnified plot of the vertical resonant peak as a function of f obtained at $h = 0 \mu\text{m}$. The solid line shows a fit to Eq. (7) with $m_v = 2.42 \times 10^{-11} \text{ g}$, $k_v = 10.02 \text{ N/m}$, and $\xi_v = 5.82 \times 10^{-7} \text{ N}\cdot\text{s/m}$. (b) A magnified plot of the horizontal resonant peak as a function of f obtained at $h = 0 \mu\text{m}$. The solid line shows a fit to Eq. (7) with $m_h = 4.09 \times 10^{-12} \text{ g}$, $k_h = 0.17 \text{ N/m}$, and $\xi_h = 1.57 \times 10^{-7} \text{ N}\cdot\text{s/m}$.

Figures 6(a) and 6(b) show respectively the magnified plots of the vertical and the horizontal resonant peaks as a function of f obtained when the fiber tip just touches the water–air interface ($h = 0 \mu\text{m}$). The solid lines are the fits to Eq. (7), which describes the data well with the two sets of fitting parameters: $m_v = 2.42 \times 10^{-11} \text{ g}$, $k_v = 10.02 \text{ N/m}$, and $\xi_v = 5.82 \times 10^{-7} \text{ N}\cdot\text{s/m}$ for the vertical resonant peak and $m_h = 4.09 \times 10^{-12} \text{ g}$, $k_h = 0.17 \text{ N/m}$, and $\xi_h = 1.57 \times 10^{-7} \text{ N}\cdot\text{s/m}$ for the horizontal resonant peak. In the fitting, two additional fitting parameters are used to describe the slow linear decay of the noise background with increasing f . This

noise background has been subtracted from the data shown in Fig. 6. Note that the vertical axes in Figs. 6(a) and 6(b) are drawn separately using the calibration constants obtained respectively for the vertical and the horizontal oscillation modes.

Figure 7 shows the fitted values of the vertical friction coefficient ξ_v (black circles) and the horizontal friction coefficient ξ_h (red triangles) as a function of the immersion length h . The error bars in the plot indicate the typical fitting uncertainties of the data. With increasing viscous damping (i.e. with increasing h), the frequency peak broadens while the peak height decreases, causing the uncertainties of the fitted values of ξ_v and ξ_h to increase with h . The experimental uncertainties of the measured ξ_v are found to be at the 10% level. The measured ξ_h has larger systematic uncertainties because the signal-to-noise ratio of the horizontal resonant peak is smaller than that of the vertical resonant peak.

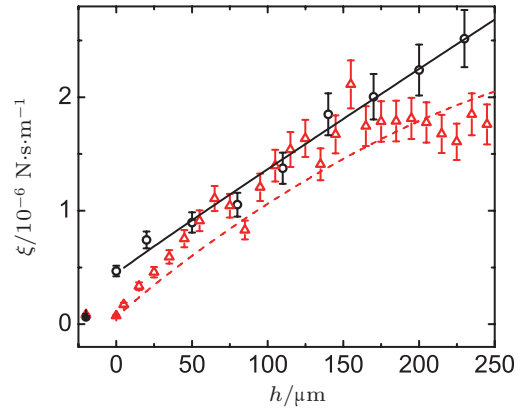


Fig. 7. Fitted values of the vertical friction coefficient ξ_v (black circles) and horizontal friction coefficient ξ_h (red triangles) as a function of the immersion length h . The measurements are made using a modified cantilever with $k \approx 10 \text{ N/m}$. For comparison, the fitted values of ξ_v and ξ_h in air (solid symbols) are also shown at $h = -20 \mu\text{m}$. The solid line is a least-square fit of Eq. (8) to the circles with $A = 4.17 \times 10^{-7} \text{ N}\cdot\text{s/m}$ and $\eta = 0.97 \text{ cP}$. The dashed line is a plot of Eq. (11) with $\eta = 0.97 \text{ cP}$.

Figure 7 reveals two interesting features of the interfacial hydrodynamics. (i) The measured ξ_v at the $h = 0$ limit ($\approx 4.7 \times 10^{-7} \text{ N}\cdot\text{s/m}$) is approximately 7.3 times larger than that measured in air ($\approx 6.45 \times 10^{-8} \text{ N}\cdot\text{s/m}$), whereas the measured ξ_h at the $h = 0$ limit ($\approx 7.5 \times 10^{-8} \text{ N}\cdot\text{s/m}$) is about the same as that measured in air ($\approx 8.4 \times 10^{-8} \text{ N}\cdot\text{s/m}$). For comparison, we include in the plot the fitted values of ξ_v and ξ_h in air. They are placed at $h = -20 \mu\text{m}$. (ii) The measured $\xi_v(h)$ as a function of h shows an approximate linear dependence on h for large values of h .

Previously, we have shown that the vertical friction coefficient ξ_v has the form^[14]

$$\xi_v = A + 1.09\xi_{\parallel}^0 + \frac{\sqrt{2}}{2}\pi dh\sqrt{\rho\omega_0\nu\eta}, \quad (8)$$

where A is a constant independent of h . The second term on the right hand side of Eq. (8) represents the zero-frequency friction coefficient. For a simple prolate spheroid of length h

and diameter d fully immersed in an infinite liquid of viscosity η , it has an analytic form^[18]

$$\xi_{\parallel}^0 = 8\pi\eta h \frac{e^3}{(1+e^2)\ln[(1+e)/(1-e)] - 2e}, \quad (9)$$

where $e = (1 - (d/h)^2)^{1/2}$ is the eccentricity of the spheroid. When $d/h = (1 - e^2)^{1/2} \ll 1$, ξ_{\parallel}^0 takes the limiting form^[18]

$$\xi_{\parallel}^0 = \frac{2\pi\eta h}{\ln(h/d) + \gamma}, \quad (10)$$

with $\gamma \simeq 0.193$. Except for the logarithmic correction factor, ξ_{\parallel}^0 (and thus ξ_v) is a linear function of h for large values of h . Equations (8) and (10) thus explain the linear behavior of the measured ξ_v at large values of h . For the long cylindrical fiber used in the experiment, the analytic form of ξ_{\parallel}^0 is not available at the moment. Our recent numerical calculation^[14] showed that equation (9) can still be used with a correction factor of 1.09.

The third term on the right hand side of Eq. (8) represents the frequency-dependent part of the friction coefficient parallel to the long axis of a long oscillating cylinder fully immersed in an infinite liquid of viscosity η and density ρ .^[12,19] It arises from the viscous boundary layer at finite oscillation frequencies. Here ω_{0v} is the oscillation frequency. The solid line in Fig. 7 is a least-square fit of Eq. (8) to the circles with A and η as two fitting parameters. It is seen that equation (8) fits the data well and the fitted value of $\eta = 0.97$ cP agrees well with the expected value for water at room temperature. It will be shown below that the constant offset $A (= 4.17 \times 10^{-7} \text{ N} \cdot \text{s}/\text{m})$ in Eq. (8) is caused by the extra friction imposed by the fluctuating contact line between the glass fiber and the water–air interface. Figure 7 clearly shows that the new hanging fiber apparatus is indeed capable of measuring a minute amount of the viscous drag produced by a (fluctuating) contact line.

Unlike the vertical oscillation of the fiber, in which the circular contact line moves along the fiber axis, the horizontal oscillation of the fiber does not involve any relative motion between the contact line and the glass fiber. As a result, there should not be a constant offset A in the horizontal friction coefficient ξ_h . Thus we fit the measured ξ_h in Fig. 7 to the equation

$$\xi_h = 2 \left(1.09\xi_{\parallel}^0 + \frac{\sqrt{2}}{2} \pi d h \sqrt{\rho \omega_{0h} \eta} \right), \quad (11)$$

where ω_{0h} is the oscillation frequency of the horizontal mode. It has been shown^[12,18] that the friction coefficient perpendicular to the axis of a long cylinder is a factor of 2 larger than that parallel to the long axis of the cylinder. Therefore, a factor of 2 is introduced in Eq. (11). The dashed line in Fig. 7 is a plot of Eq. (11) with $\eta = 0.97$ cP, which describes the data relatively well.

Unlike the vertical resonant frequency ω_{0v} , which does not change much with increasing h , the horizontal resonant

frequency ω_{0h} changes significantly from $2\pi \times 30$ kHz to $2\pi \times 14$ kHz when the immersion length h is changed from 0 to 250 μm . The horizontal frequency ω_{0h} in Eq. (11) is therefore treated as a function of h , rather than a constant as in the case for ω_{0v} . This large change in ω_{0h} together with the small signal-to-noise ratio of the horizontal resonant peak introduces relatively large errors to the measured ξ_h at large values of h . These larger errors explain the deviations between the data and the dashed line in Fig. 7. Note that the measured ξ_h at the $h = 0$ limit has the smallest error and figure 7 clearly demonstrates that the intercept of the measured ξ_h is close to zero, which is beyond the experimental uncertainties.

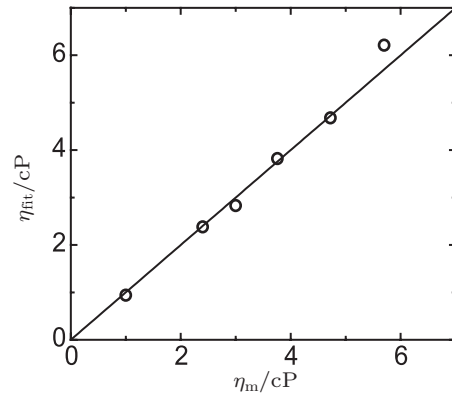


Fig. 8. Comparison of the fitted values of the fluid viscosity η_{fit} with the fluid viscosity η_m directly measured using a commercial rheometer. The solid line indicates $\eta_{\text{fit}} = \eta_m$.

To further test the capability of the hanging fiber apparatus, we repeat the measurements of ξ_v at the interface using aqueous solutions of glycerine with varying mass concentrations from 0 wt% (pure water) to 50 wt%. For each aqueous solution of glycerine at a fixed mass concentration, we measure ξ_v as a function of h , as shown in Fig. 7, from which we obtain the fitted value of η_{fit} . Figure 8 compares the obtained values of η_{fit} with the fluid viscosity η_m directly measured using a commercial rheometer (model ARES, Thermal Analysis Instrument). The solid line indicates $\eta_{\text{fit}} = \eta_m$. Figure 8 thus demonstrates that our measurements of the friction coefficient using the hanging fiber are accurate.

4.2. Measurement of friction resulting from a fluctuating contact line

To further investigate the contact line's contribution to the friction coefficient (i.e. the intercept of the measured ξ_v), one needs to measure ξ_v at the $h = 0$ limit so that the second and the third terms on the right hand side of Eq. (8) can be neglected. In the experiment, we move the glass fiber downward from the air to the liquid interface. When the fiber tip touches the interface, the AFM detects a large capillary force. After touching the interface, the glass fiber is pulled back slightly ($\sim 10 \mu\text{m} = 2d$) to a position just before it detaches the interface. In this way, the contribution of the bulk fluid to the

measured ξ_v (and ξ_h) is minimized. The fiber is then kept stationary and the thermal power spectrum $|z(f)|^2$ is measured repeatedly for different fluid interfaces with the fluid viscosity η varied in the range of 0.3–20 cP.

The liquid samples used are given in Table 4. The glass fiber used in the experiment is coated with a monolayer of trichloro(1H, 1H, 2H, 2H-perfluorooctyl)silane (FTS) with diameter $d = 5 \mu\text{m}$. In one set of measurements, organic liquids and silicone oil are used to cover the above mentioned viscosity range. No contact angle hysteresis is observed in this system and the equilibrium contact angle is $\theta_0 = 0^\circ$. In the other set of measurements, glycerine–water solutions with different mass concentrations are used to cover the viscosity range. This system shows a contact angle hysteresis with the advancing angle $\theta_a = 95^\circ$ and the receding angle $\theta_r = 70^\circ$. The values of the contact angle θ are determined by using the hanging fiber probe to directly measure the capillary force, $f = \pi d \gamma \cos(\theta)$, for different liquid–air interfaces at 25 °C. Here πd is the contact line length and γ is the surface tension.

Table 4. Liquid samples used and values of their viscosity η , density ρ , surface tension γ , and advancing/receding contact angles θ_a/θ_r for the glass fiber coated with a monolayer of FTS. The contact angles were measured using the AFM-based hanging fiber probe.

Fluids	η/cP	$\rho/\text{g}\cdot\text{cm}^{-3}$	$\gamma/\text{mN}\cdot\text{m}^{-1}$	$\theta_a/\theta_r/(^\circ)$
Hexane	0.29	0.66	18	0
Octane	0.52	0.70	21	0
Decane	0.86	0.73	24	0
Hexadecane	3.0	0.77	27	0
Silicone oils	5–20	~ 1.0	~ 21	0
Glycerine + water	1–20	1.0–1.2	72–66	95/70

The measured ξ_v has three contributions, $\xi_v = \xi_v^a + \xi_v^b + \xi_v^c$, where ξ_v^a is the contribution from the air, as a large portion of the glass fiber and the entire cantilever are exposed in the air. This term can be measured separately before the fiber touches the interface. The second term ξ_v^b is the contribution from the bulk fluid. The third term ξ_v^c is the contribution from the moving contact line. The measured ξ_h contains only two contributions, $\xi_h = \xi_h^a + \xi_h^b$, and the contact line contribution ξ_h^c to the horizontal oscillation is zero, because there is no relative motion between the glass fiber and the contact line.

While we have tried to reduce the bulk contribution term ξ_v^b as much as we could in the experiment, the oscillating fiber still feels the drag on its end surface and sidewall due to a small capillary rise of the wetting fluid around the fiber tip, as indicated in Fig. 1(b). Therefore, one can write $\xi_v^b = \xi_v^e + \xi_v^s$, where ξ_v^e is the contribution from the end surface and ξ_v^s is the contribution from the sidewall. For a circular end surface, ξ_v^e can be calculated analytically and the final results are given in Appendix A. The calculation of ξ_v^s is somewhat complicated, because the meniscus of the liquid interface near the contact line is a curved surface. Below we discuss two limiting cases

in which $\xi_v^s \simeq 0$, and leave the details about how to estimate ξ_v^s for a finite capillary rise in Appendix A.

The meniscus of the liquid interface around a stationary fiber has the form^[20]

$$z = b \left[\ln \left(\frac{2\ell_c}{b} \right) - \ln \left[\frac{r}{b} + \left[\left(\frac{r}{b} \right)^2 - 1 \right]^{1/2} \right] \right], \quad (12)$$

where z is the meniscus height, r is its radial location, $\ell_c = \sqrt{\gamma/\rho g}$ is the capillary length, and $b = (d/2) \cos \theta$. Here ρ is the fluid density, g is the gravitational acceleration, and d is the fiber diameter. For large contact angles ($\theta \approx 90^\circ$), we have $b \approx 0$ and thus the capillary rise is negligibly small. In this case, we have $\xi_v^s \approx 0$. For small contact angles ($\theta \approx 0^\circ$), however, we have $b \approx (d/2)$ and the height of the capillary rise on the fiber ($r = d/2$) is $z_0 \simeq (d/2) \ln(4\ell_c/d) \approx 3.6d$ for an organic liquid interface with $\ell_c \simeq 1.7 \text{ mm}$ (and $d = 5 \mu\text{m}$). The liquid film thickness δr around the fiber tip varies with the meniscus height z and has a typical value of $\sim 1.9d$ at one-third of the height of the capillary rise.

As illustrated in the inset of Fig. 1(b), a moving contact line (MCL) involves fluid motion (i) at a small distance a ($\sim 1 \text{ nm}$) in the immediate vicinity of the contact line, in which the molecular interactions between the liquid and the solid are important, and (ii) in the “outer region” of meso- or macroscopic size ℓ , in which classical hydrodynamics are applicable. When the fiber oscillates, the viscous shear wave can only penetrate into a thin fluid layer of thickness $\lambda = (2\nu/\omega_0)^{1/2}$ from the fiber surface,^[19] where $\nu = \eta/\rho$ is the kinematic viscosity. The capillary rise (i.e. the fluid in regime (ii) marked as a wedge-shaped fluid layer in the inset of Fig. 1(b)) will oscillate in phase with the fiber, contributing only an extra mass and no dissipation to the oscillating fiber, if its thickness δr is smaller than λ . Hence in this case we again have $\xi_v^s \approx 0$.

For liquids with $\eta \gtrsim 1 \text{ cP}$, $\omega_{0v} \simeq 2\pi \times 100 \text{ kHz}$ and $\omega_{0h} \simeq 2\pi \times 30 \text{ kHz}$, we have $\lambda_v \gtrsim 1.8 \mu\text{m}$ and $\lambda_h \gtrsim 3.3 \mu\text{m}$. By choosing a thin glass fiber with $d \lesssim 2 \mu\text{m}$, one can thus reduce the sidewall contribution and set $\xi_v^s \approx 0$. The above discussion is valid only for the fluid layer with a non-slip boundary condition (i.e. in regime (ii)). As a result, the oscillating fiber only feels the drag on its end surface and the MCL in regime (i), where the wall velocity slips as demonstrated by the previous MD simulations^[21–23] and by recent continuum hydrodynamic calculations.^[23,24] Such a slip produces a relative motion between the contact line and the oscillating fiber along its axis and thus gives rise to the contact-line friction term ξ_v^c . After subtracting the air and the end-surface contributions ξ_v^a and ξ_v^e , we find that the resulting friction coefficients, $\xi_v^c \equiv \xi_v - \xi_v^a - \xi_v^e$ and $\xi_h^c \equiv \xi_h - \xi_h^a - \xi_h^e$, for fluids with different contact angles θ all collapse onto two separate master curves.

Figure 9 shows the obtained friction coefficients ξ_v^c (black open symbols) and ξ_h^c (red open symbols) as a function of

fluid viscosity η . The measured ξ_h^c shows no apparent dependence on η and can be described by the equation $\xi_h^c = B_h$ with $B_h = 0.5 \times 10^{-7} \text{ N}\cdot\text{s}/\text{m}$ (lower (red) solid line). The constant term B_h characterizes the internal dissipation of the hanging fiber and thus is a device parameter.^[25] This result further confirms our expectation that there is no contact line contribution remaining in the measured ξ_h^c .

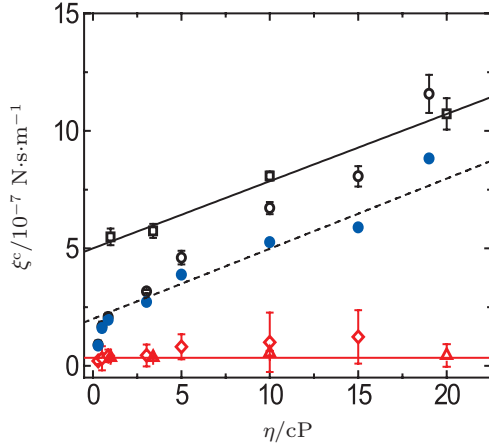


Fig. 9. Obtained friction coefficients ξ_v^c (black open symbols) and ξ_h^c (red open symbols) as a function of fluid viscosity η . The circles and diamonds are obtained for organic liquids with $\theta_0 = 0^\circ$, and the squares and triangles are obtained for the glycerine–water solutions with $\theta_a = 95^\circ$. The upper (black) solid line is a fit of Eq. (13) to the squares with $B_v = 5.1 \times 10^{-7} \text{ N}\cdot\text{s}/\text{m}$ and $\alpha = 1.82 \pm 1$. The lower (red) solid line shows the fitted constant line, $\xi_h^c = 0.5 \times 10^{-7} \text{ N}\cdot\text{s}/\text{m}$. The blue solid circles are obtained from the open circles after a subtraction of the sidewall friction ξ_v^s due to the capillary rise on the glass fiber (see text). The dashed line is a linear fit of Eq. (13) to the blue solid circles with $\alpha = 1.9 \pm 1$ and $B_v = 2.0 \times 10^{-7} \text{ N}\cdot\text{s}/\text{m}$.

It is also found that the measured ξ_v^c can be described by a universal function

$$\xi_v^c = B_v + \alpha\pi d\eta, \quad (13)$$

where πd is the contact line length and B_v is the device parameter associated with the vertical mode. The upper (black) solid line shows a fit to the squares with $B_v = 5.1 \times 10^{-7} \text{ N}\cdot\text{s}/\text{m}$ and $\alpha = 1.82 \pm 1$. This set of data has an advancing angle $\theta_a = 95^\circ$ and thus the effect of the capillary rise to the measured ξ_v^c is minimal ($\xi_v^s \approx 0$).

For the open circles, however, their contact angle $\theta_0 = 0^\circ$ and the liquid film thickness δr around the fiber tip is $\delta r \approx 9.5 \mu\text{m}$ for a fiber with $d = 5 \mu\text{m}$. This value of δr is much larger than the penetration depth of the vertical mode $\delta_v \approx 1.8 \mu\text{m}$. Thus a contribution from the sidewall ξ_v^s has to be subtracted out from the measured ξ_v^c . In Appendix A, we make an estimate of the sidewall friction ξ_v^s due to the capillary rise on the glass fiber used in the experiment and find that $\xi_v^s \approx 0.92\pi d\eta$. The blue solid circles in Fig. 9 are obtained when this correction is applied to the open circles. The dashed line is a fit of Eq. (13) to the blue solid circles with $\alpha = 1.9 \pm 1$ and $B_v = 2.0 \times 10^{-7} \text{ N}\cdot\text{s}/\text{m}$. The value of B_v is found to vary

with the contact angle, as the hanging fiber is under different capillary forces.

The obtained values of α are close to those obtained in a recent experiment using a single-mode mechanical resonator.^[25] In that experiment, thinner glass fibers with diameter $d \lesssim 2 \mu\text{m}$ were used, so that the friction contribution from the capillary rise was eliminated ($\xi_v^s \simeq 0$) and the resulting value of α ($= 0.8 \pm 0.2$) had smaller experimental uncertainties. In the present experiment, however, we use a larger diameter fiber ($d = 5 \mu\text{m}$) in order to excite both the vertical and the horizontal resonant modes. The use of a thicker fiber introduces larger uncertainties in the obtained value of α because of the uncertainties in the subtraction of the sidewall friction ξ_v^s due to the capillary rise on the hanging fiber. Nonetheless, figure 9 clearly reveals two distinct behaviors between the longitudinal friction ξ_v^c along the fiber axis and the traversal friction ξ_h^c perpendicular to the fiber axis and thus demonstrates that ξ_v^c given in Eq. (13) is indeed associated with a fluctuating (and slipping) contact line in regime (i).

de Gennes *et al.*^[20] has calculated the friction coefficient ξ_v^d for fluid motion in regime (ii) away from the contact line, in which the classical hydrodynamics are applicable. The obtained ξ_v^d has the form^[20]

$$\xi_v^d \simeq (3\ln(\ell/a)/\theta)\pi d\eta, \quad (14)$$

where the contact angle θ is assumed to be small and a cut-off length a (see the inset of Fig. 1(b)) is introduced to avoid the dissipation divergence of the MCL. The calculated ξ_v^d in Eq. (14) becomes $\xi_v^d \simeq (26/\theta)\pi d\eta$ for $\ell \simeq 6 \mu\text{m}$. This value of ξ_v^d is about 100 times larger than the measured ξ_v^c for liquids with $\theta \simeq 15^\circ$ and even becomes divergent for liquids with $\theta = 0^\circ$. Clearly, the calculated ξ_v^d for fluid motion in regime (ii) does not apply to the measured ξ_v^c shown in Fig. 9, further confirming that ξ_v^c given in Eq. (13) is directly connected to the motion of a fluctuating (and slipping) contact line in regime (i). There is a physical reason for the absence of de Gennes' ξ_v^d in region (ii) away from the contact line. This is because the amplitude of the partial slip between the fluid and the solid is so small at thermal equilibrium that its magnitude is less than the thermal vibration amplitude of the solid atoms. Hence we can impose a cutoff distance from the contact line so that de Gennes' ξ_v^d in region (ii) is beyond the cutoff and therefore can be neglected.^[26]

The establishment of the scaling law $\xi_v^c = \alpha\pi d\eta$ for the contact line dissipation has several important implications. First, as a universal scaling law applicable to liquids with different viscosities and contact angles, it provides a rigorous relationship which can be used to test various microscopic models for the MCL. Second, it sets up an intrinsic bound for the dissipation of the MCL in regime (i), which is useful for evaluating relevant molecular parameters associated with the MCL,

such as the slip length for different fluids. Finally, the understanding of the contact line dissipation also provides a solid foundation for the further study of other liquid interfaces of practical interest, such as those coated with polymers, surfactant, and lipids.

5. Conclusion

We have developed a dual-mode mechanical resonator using an atomic force microscope (AFM) as a force sensor. The resonator consists of a long vertical glass fiber with one end glued onto a rectangular cantilever beam and the other end immersed through a liquid–air interface. Typical dimensions of the glass fiber used are 4 μm in diameter and 270 μm in length. With a proper amount of glue and a suitable aspect ratio of the glass fiber, we are able to detect two resonant modes associated with the vertical oscillation of the cantilever and the horizontal swing of the hanging fiber. The measured resonant spectrum $|z(f)|^2$ of vertical deflections of the cantilever is extremely sensitive to a minute amount of viscous damping due to the hydrodynamic interactions between the hanging fiber and the liquid–air interface. Such hydrodynamic interactions may give rise to a dissipative or viscoelastic response of the fluid interface to the strain imparted by thermal fluctuations of the hanging fiber probe.

The dual-mode mechanical resonator is tested by the measurement of the longitudinal friction coefficient ξ_v^c along the fiber axis and the traversal friction ξ_h^c perpendicular to the fiber axis. From the two distinct behaviors between the measured ξ_v^c and ξ_h^c , we demonstrate that ξ_v^c is indeed associated with a fluctuating (and slipping) contact line in regime (i). By varying the liquid viscosity η for almost two decades, we find that the contact line dissipation obeys a scaling law, $\xi_v^c = \alpha\pi d\eta$, where πd is the contact line length and $\alpha = 1.82 \pm 1$, which does not change much with the liquid–solid contact angle. This universal scaling law applicable to liquids with different viscosities, surface tensions, and contact angles establishes a rigorous relationship that can be used to test various microscopic models for the MCL.

The new technique has several important advantages. (i) Because only a thin fiber tip is in contact with the liquid, the motion of the AFM cantilever is not over-damped by the fluid viscosity. Consequently, the resonant peaks have a relatively large value of quality factor Q , resulting in a high sensitivity to small changes in viscous damping. Therefore, the technique can be used to measure the fluid viscosity over a wide range for samples with a small volume. (ii) The use of a thin hanging fiber as a probe provides a simple geometry for the quantitative analysis of the rheological property of complex fluids near the interface. It provides ample flexibilities for varying the surface chemistry of the hanging fiber and the wetting property of

the fluids to be studied, making the technique particular useful for the investigation of the contact line dynamics. (iii) In addition, with the capability of simultaneously measuring the longitudinal friction along the fiber axis and the traversal friction perpendicular to the fiber axis, the technique provides a convenient method for the study of the rheological property of anisotropic fluids, such as liquid crystals. (iv) This technique has the advantages of a commercial AFM with fast sampling rate up to 5 MHz, precise control of the vertical motion of the cantilever down to nanometers, and ease of operation with a user-friendly computer interface. It only takes 1–3 min to collect a power spectrum with adequate frequency resolution and signal-to-noise ratio.

The dual-mode mechanical resonator provides a powerful tool for the study of interfacial hydrodynamics, by which various liquid interfaces coated with polymers, surfactants, and biomolecules (i.e. membranes) may be characterized at a quantitative level and with a precise control of length scales and surface chemistry. The present study represents the first step toward this direction.

Appendix A: Calculation of the friction coefficient resulting from the bulk fluid

The friction coefficient resulting from the end surface of the fiber tip can be estimated with the friction coefficient ξ^{disk} for an oscillating disk of diameter d fully immersed in an unbounded liquid. The values of ξ_v^{disk} and ξ_h^{disk} for the parallel and the perpendicular components of ξ^{disk} relative to the normal direction of the disk are known.^[27,28] Therefore, we have

$$\xi_v^e \simeq \frac{1}{2} \xi_v^{\text{disk}} = 4d\eta + \frac{8\sqrt{2}}{3\pi} d^2 \sqrt{\rho\omega_{0v}\eta}, \quad (\text{A1})$$

$$\xi_h^e \simeq \frac{1}{2} \xi_h^{\text{disk}} = \frac{8}{3} d\eta + \frac{32\sqrt{2}}{27\pi} d^2 \sqrt{\rho\omega_{0h}\eta}, \quad (\text{A2})$$

where ω_{0v} and ω_{0h} are the oscillation frequencies of the vertical and the horizontal resonant modes, respectively. The factor of 1/2 is introduced in the second equality of Eqs. (A1) and (A2) because the fiber has only one (circular) end surface in contact with the liquid.

The above results are for an oscillating disk with zero thickness. For an oscillating disk with a finite thickness, numerical results are available^[29] for different aspect ratios $\Gamma = h/d$, where h is the thickness and d is the diameter of the disk. It was found^[26] that the friction coefficient for an oscillating disk of varying aspect ratio Γ with fixed values of $d = 1.5 \mu\text{m}$, $\eta = 1.76 \text{ cP}$, and $\omega_0 = 2\pi \times 130 \text{ kHz}$ can be well described by the equation

$$\xi_v^{\text{disk}} = \xi_v^e + \xi_v^s = (3.27 + 1.74\Gamma)\pi d\eta, \quad (\text{A3})$$

where ξ_v^e is the contribution from the two end surfaces of the disk^[27,28] and ξ_v^s is the contribution from the sidewall. To

estimate the sidewall friction ξ_v^s of the capillary rise on the glass fiber used in the experiment (with $d = 5 \mu\text{m}$), we assume that the sidewall friction for the bottom one-third of the capillary rise ($h = (3.6 - 2)d/3 = 0.53d$) with a curved meniscus (see Fig. 1(b)) is equivalent to that of an oscillating disk with $\Gamma \approx 0.53$ fully immersed in an unbounded liquid. In this case, we have $\xi_v^s \approx 0.92\pi d\eta$.

Acknowledgements

We have benefited from illuminating discussions with Qian T Z, Wang X P, and Beck D.

References

- [1] Horber J K and Miles M J 2003 *Science* **302** 1002
- [2] Yum K, Wang N and Yu M F 2010 *Nanoscale* **2** 363
- [3] Roters A, Gelbert M, Schimmel M, Rhe J and Johannsmann D 1997 *Phys. Rev. E* **56** 3256
- [4] Roters A, Schimmel M, Rhe J and Johannsmann D 1998 *Langmuir* **14** 3999
- [5] Delmas M, Monthieux M and Ondarcuhu T 2011 *Phys. Rev. Lett.* **106** 136102
- [6] Rajagopalan R 2000 *Colloids and Surfaces A* **174** 253
- [7] Chen G Y, Warmack R J, Thundat T, Allison D P and Huang A 1994 *Rev. Sci. Instrum.* **65** 2532
- [8] Sader J E 1998 *J. Applied Phys.* **84** 64
- [9] Clarke R J, Jensen O E, Billingham J, Pearson A P and Williams P M 2006 *Phys. Rev. Lett.* **96** 050801
- [10] Paul M R and Cross M C 2004 *Phys. Rev. Lett.* **92** 235501
- [11] Paul M R, Clark M T and Cross M C 2006 *Nanotechnology* **17** 4502
- [12] Ma H L, Jimenez J and Rajagopalan R 2000 *Langmuir* **16** 2254
- [13] Mehta A, Cherian S, Hedden D and Thundata T 2001 *Appl. Phys. Lett.* **78** 1637
- [14] Xiong X, Guo S, Xu Z, Sheng P and Tong P 2009 *Phys. Rev. E* **80** 061604
- [15] Slaughter W S 2002 *The Linearized Theory of Elasticity* (Boston: Birkhauser)
- [16] Butt H J and Jaschke M 1995 *Nanotechnology* **6** 1
- [17] Reif F 1985 *Fundamentals of Statistical and Thermal Physics* (Auckland: McGraw-Hill)
- [18] Leal L G 2007 *Advanced Transport Phenomena* (Cambridge: Cambridge University Press) p. 557
- [19] Landau L D and Lifshitz E M 1987 *Fluid Mechanics* (2nd edn.) (Oxford: Butterworth-Heinemann)
- [20] de Gennes P G, Brochard-Wyart F and Qur D 2004 *Capillarity and Wetting Phenomena* (New York: Springer) p. 142
- [21] Koplik J, Banavar J R and Willemsen J F 1988 *Phys. Rev. Lett.* **60** 1282
- [22] Thompson P A and Robbins M O 1989 *Phys. Rev. Lett.* **63** 766
- [23] Qian T Z, Wang X P and Sheng P 2004 *Phys. Rev. Lett.* **93** 094501
- [24] Qian T Z, Wang X P and Sheng P 2006 *J. Fluid Mech.* **564** 333
- [25] Guo S, Gao M, Xiong X M, Wang Y J, Wang X P, Sheng P and Tong P 2013 *Phys. Rev. Lett.* **111** 026101
- [26] Guo S, Gao M, Xiong X M, Wang Y J, Wang X P, Sheng P and Tong P 2013 *Phys. Rev. Lett.* **111** 026101 (supplemental material)
- [27] Williams W E 1966 *J. Fluid Mech.* **25** 589
- [28] Zhang W and Stone H A 1998 *J. Fluid Mech.* **367** 329
- [29] Loewenberg M 1993 *Phys. Fluids A* **5** 3004